HHS Public Access

Author manuscript

Glia. Author manuscript; available in PMC 2016 December 07.

Published in final edited form as:

Glia. 2015 January ; 63(1): 91–103. doi:10.1002/glia.22735.

Ciliary neurotrophic factor (CNTF) activation of astrocytes decreases spreading depolarization susceptibility and increases potassium clearance

Jessica L. Seidel[1,5], **Mathilde Faideau**[2,3], **Isamu Aiba**[1], **Ulrike Pannasch**[4,6], **Carole Escartin**[2,3], **Nathalie Rouach**[4], **Gilles Bonvento**[2,3], and **C. William Shuttleworth**[1]

[1] Dept. Neurosciences, University of New Mexico School of Medicine, Albuquerque NM, USA

[2] CEA, I2BM, MIRCen, Fontenay-aux-Roses, France

[3] URA CEA CNRS 2210, Fontenay-aux-Roses, France

[4] CIRB, INSERM U1050, CNRS UMR 7241, Collège de France, 75005 Paris, France.

Abstract

Waves of spreading depolarization (SD) have been implicated in the progressive expansion of acute brain injuries. SD can persist over several days, coincident with the time course of astrocyte activation, but little is known about how astrocyte activation may influence SD susceptibility. We examined whether activation of astrocytes modified SD threshold in hippocampal slices. Injection of a lentiviral vector encoding Ciliary neurotrophic factor (CNTF) into the hippocampus *in vivo*, led to sustained astrocyte activation, verified by up-regulation of glial fibrillary acidic protein (GFAP) at the mRNA and protein levels, as compared to controls injected with vector encoding LacZ. In acute brain slices from LacZ controls, localized 1M KCl microinjections invariably generated SD in CA1 hippocampus, but SD was never induced with this stimulus in CNTF tissues. No significant change in intrinsic excitability was observed in CA1 neurons, but excitatory synaptic transmission was significantly reduced in CNTF samples. mRNA levels of the predominantly astrocytic Na^+/K^+-ATPase pump α2 subunit were higher in CNTF samples, and the kinetics of extracellular K^+ transients during matched synaptic activation were consistent with increased K^+ uptake in CNTF tissues. Supporting a role for the Na^+/K^+-ATPase pump in increased SD threshold, ouabain, an inhibitor of the pump, was able to generate SD in CNTF tissues. These data support the hypothesis that activated astrocytes can limit SD onset via increased K^+ buffering capacity and suggest that therapeutic strategies targeting these glial cells could improve the outcome following acute brain injuries associated with SD.

Corresponding Author: C.W. Shuttleworth, MSC08 4740, 1 University of New Mexico, Albuquerque, NM 87131-0001, BShuttleworth@salud.unm.edu, 505-272-4290.

[5]Present address: Department of Radiology, Neurovascular Research Laboratory, Massachusetts General Hospital, Harvard Medical School, Charlestown, Massachusetts, USA

[6]Present address: Neuroscience Research Center, Charité-Universitätsmedizin, 10117 Berlin, Germany.

Financial Disclosure:

The funders had no role in study design, data collection and analysis, decision to publish, or preparation of the manuscript

AUTHOR CONTRIBUTIONS

Performed experiments and analyzed data: JLS, MF, IA, UP, CE, GB, CWS; Conceived experiments, interpreted data and wrote manuscript: JLS, NR, CE, GB, CWS.

Keywords

Ciliary neurotrophic factor (CNTF); Spreading depression; Hippocampus; astrocyte activation; brain slice

INTRODUCTION

Spreading depolarizations (SD) are slowly propagating waves of near-complete neuronal and glial depolarization that are mediated by the progressive accumulation of K^+ and/or glutamate in the extracellular space (Leao 1944; Somjen 2001). SD can be generated by a variety of stimuli, including intense localized electrical stimulation, K^+ application, mechanical injury or ischemia. If SD is generated in otherwise healthy tissue, neuronal ionic gradients and function can be fully restored (Leao 1944; Nedergaard and Hansen 1988). However, SDs that occur in the context of ischemia or experimental deprivation of oxygen and glucose are associated with neuronal injury, in both animal models (Hartings et al. 2003; Hossmann 1996; Nedergaard and Astrup 1986; Strong et al. 2000) and in human trauma and stroke (Dohmen et al. 2008; Fabricius et al. 2006; Hartings et al. 2011). For these reasons, there is significant interest in approaches that can limit the onset of SD (Dreier 2011; Lauritzen et al. 2011).

Astrocytes depolarize during the propagation of an SD wave (Somjen 2001), and their function is likely important for regulating SD and its deleterious consequences in pathophysiological states (Charles and Brennan 2009; Leis et al. 2005; Risher et al. 2012). Selective inhibition of astrocyte metabolism, with the toxin fluoroacetate (FAc), accelerates SD onset (Largo et al. 1996; Largo et al. 1997; Lian and Stringer 2004), and prolonged exposure to FAc alone initiates SD in acute brain slices, accompanied by irreversible neuronal injury (Canals et al. 2008). In addition, astrocyte glycogen stores appear to contribute to determining the propagation rate of SD (Seidel and Shuttleworth 2011). Disruption of extracellular K^+ and/or glutamate homeostasis could underlie these effects.

It is well appreciated that astrocytes are not a static population of cells, and can undergo substantial changes in structure and function due to a wide range of stimuli. Transformation to an “activated” phenotype has been described following brain injury, and involves marked up-regulation of the structural proteins glial fibrillary acidic protein (GFAP), nestin, and vimentin (Kalman 2004; Pekny and Nilsson 2005). Repetitive SD events can increase GFAP expression in astrocytes (Kraig et al. 1991; Wiggins et al. 2003), and it was more recently shown that inducing SD daily *in vivo* was associated with increased GFAP expression, as well as an increased threshold for SD generation (Sukhotinsky et al. 2011). It is not yet known whether astrocyte activation alone modifies SD susceptibility, but this could be important following many forms of injury where astrocyte activation and SD occur coincidently.

Whether activated astrocytes contribute to damage or neuroprotection has been difficult to determine, probably because there is significant heterogeneity in the functional changes associated with astrocyte activation depending on the activation stimulus (Escartin and Bonvento 2008). Recent studies have begun to explore the functional roles of astrocytes

following their selective activation by ciliary neurotrophic factor (CNTF). CNTF is a cytokine related to the interleukin-6 family that displays neurotrophic and differentiating effects over cells in the central nervous system (Lin et al. 1989). *In vitro* stimulation with CNTF leads to astrocyte activation (Hudgins and Levison 1998), and this has been extended to *in vivo* studies by exploiting lentiviral infection of neurons to constitutively express and release CNTF (Escartin et al. 2006; Escartin et al. 2007). We here examine whether astrocytes activated by CNTF might significantly change SD threshold in acute brain slice preparations. The results demonstrate persistent activation of hippocampal astrocytes following lentiviral-mediated gene delivery of CNTF *in vivo*. In addition, a large elevation in SD threshold was observed in subsequent *ex vivo* slice studies, possibly due to enhanced extracellular K^+ clearance by CNTF-activated astrocytes. These findings suggest that some forms of astrocyte activation could strongly influence the spread of SD events in injured brain tissue.

MATERIALS AND METHODS

1. In vivo CNTF expression

Expression and release of CNTF in the mouse hippocampus *in vivo* was achieved by adaptation of a gene transfer approach previously described for rat striatum (Escartin et al. 2006; Escartin et al. 2007). Self-inactivated lentivirus encoding the human CNTF gene with the export sequence of Ig (lenti-CNTF), were constructed, purified and titrated as previously described (de Almeida et al. 2001). Bilateral hippocampal injections (1 μl per hippocampus at 0.1 μl/min) were made in male C57Bl/6 mice, aged 5-7 weeks using the following stereotactic coordinates: anteroposterior −2 mm from bregma; lateral +/−2 mm; ventral 1.3 mm. All experimental procedures were performed in strict accordance with the recommendations of the European Commission (86/609/EEC) concerning the care and use of laboratory animals and animals were used within 21 weeks of age. Throughout the study, an equal number of age-matched control animals were studied. These controls were injected with lentivirus encoding the β-galactosidase gene (lenti-LacZ) at the same time as injection of CNTF animals. Equal numbers of CNTF and LacZ experiments were interleaved throughout the course of the study.

Immunohistochemical detection of β-galactosidase was used to determine the distribution of transgene expression in a sample of LacZ control animals (see Figure 1A). Following perfusion fixation (4% paraformaldehyde), brains were post-fixed overnight, cryoprotected with 30% sucrose and then sectioned at 30 μm thickness using a freezing sliding knife microtome. Floating sections were permeabilized (0.1% Triton X-100), blocked (5% normal donkey serum) and incubated with mouse anti-β-galactosidase antibody (1:100, University of Iowa Developmental Studies Hybridoma Bank, overnight at 4° C) and antigen then localized with FITC-conjugated secondary antibody (1:250; Jackson ImmunoResearch Laboratories, West Grove, PA).

2. Reverse transcriptase - quantitative polymerase chain reaction (RT-qPCR)

Mice injected bilaterally with lenti-LacZ (n=6) or lenti-CNTF (n=6) in the hippocampus were sacrificed 6 weeks post-infection. The whole hippocampus was rapidly collected on ice

and stored in RNAlater (Sigma) at 4°C, until further processing. Total RNA was isolated from samples with Trizol (Invitrogen) and treated with RQ1 DNase (Invitrogen). cDNA was synthesized from 400 ng of total RNA and random primers using the SuperScript® VILO™ cDNA Synthesis Kit (Invitrogen). Samples were analyzed in triplicate by real-time PCR using the Platinum® SYBR® Green qPCR SuperMix-UDG kit (Invitrogen) and the MasterCycler® ep *realplex* (Eppendorf). A dissociation step was included to confirm the amplification of a single product. The following primers were designed with the Oligo6 software:

For each set of primers, the efficiency of the amplification reaction was measured using a 4 fold dilution standard curve, and found to be between 84% and 105%. Controls with no template and no reverse-transcriptase were included. The abundance of the gene of interest was normalized to the abundance of the housekeeping gene *Cyclophilin A* using the ΔCt method (Livak and Schmittgen 2001). *Cyclophilin A* mRNA levels were not different between the two groups.

3. Acute brain slice preparation

Acute brain slice preparation was performed as previously described (Seidel and Shuttleworth 2011), following procedures authorized by the University of New Mexico Animal Care and Use Committee. Briefly, mice were deeply anesthetized with a mixture of ketamine and xylazine, brains removed and cooled in an ice-cold cutting solution (containing, in mM: 2 KCl, 1.25 NaH_2PO_4, 6 $MgSO_4$, 26 $NaHCO_3$, 0.2 $CaCl_2$, 10 glucose, 220 sucrose and 0.43 ketamine), hemisected and then coronal slices cut at 250 or 350 μm using a Vibratome. After recovery for 1 hour at 34°C in ACSF (containing, in mM: 126 NaCl, 2 KCl, 1.25 NaH_2PO_4, 1 $MgSO_4$, 26 $NaHCO_3$, 2 $CaCl_2$, and 10 glucose, equilibrated with 95% O_2 / 5% CO_2), the ACSF was changed and slices were held at room-temperature (~23°C) until transfer to the recording chamber. Individual slices were then superfused with oxygenated ACSF at 2 ml/min at 32 or 35°C and recordings made from the hippocampal CA1 region. For *in vitro* studies, numbers refer to the number of slices, with a maximum of three slices from an individual animal used for each experimental condition.

The degree of astrocyte activation was assessed by GFAP immunohistochemistry in the same slices as used for electrophysiological studies. Slices were not re-sectioned, and extended antibody incubation periods were required for adequate penetration into the slice, using methods previously described (Hoskison and Shuttleworth 2006). Briefly, slices were fixed (4% paraformaldehyde), blocked (10% normal goat serum) and exposed to mouse anti-GFAP-Cy3 (1:200; 48 hr at 4°C, Sigma Aldrich). After thorough washing, nuclei were labeled with DAPI (300 nM, 10 min, Invitrogen, Carlsbad, CA) and slices were mounted with Gel Mount and examined using a Zeiss 510 Meta confocal microscope (Carl Zeiss, Thornwood, NY, USA). Astrocyte counts were made of GFAP and DAPI positive soma within the region of interest in the CA1 stratum radiatum, from an image stack (300×300 μm, 20 μm depth) centered above the apex of the upper blade of the dentate gyrus. Identical image acquisition parameters were used for each preparation, and the experimenter was blinded. In some studies, dendritic density was assessed by using microtubule associated protein-2 (MAP2) immunohistochemistry as previously described (Hoskison and

Shuttleworth 2006). After fixation and washing, thick slices were incubated in anti-MAP2 antibody (AP-20; 1:500, for 48 hr at 4°C), and the primary antibody localized using anti-FITC (1:200; 24 hours at 4°C).

4. Postsynaptic potentials and intracellular recordings

Excitatory post synaptic potentials (fEPSPs) were characterized following stimulation of Schaffer collateral inputs. A bipolar electrode (25 μm tip) was used to apply single shocks (80 μs pulse, 10 s interpulse interval, 0.0-0.32 mA, using a constant-current stimulus isolation unit Isoflex, AMPI, Israel) and fEPSPs were recorded using extracellular glass microelectrodes placed in stratum radiatum, ~150 μm from the pyramidal cell body layer. Recording electrodes were 3-5 MΩ when filled with ACSF. For tests of drug action, the stimulus intensity for test pulses was chosen as 50% of maximal amplitude, based on input/output curves generated in each slice.

Characterization of CA1 membrane properties were made from intracellular recordings using sharp microelectrodes (~100 MΩ when filled with 3 M KCl) as previously described (Shuttleworth and Connor 2001). Impalements were accepted if neurons required less than 100 pA of negative current injection to maintain stable resting membrane potentials more negative than −65 mV, and injection of depolarizing current pulses produced activation potentials that overshot 0 mV. After stable impalements were achieved, neurons were allowed to recover at least 10 min before characterization of input resistance, action potential threshold and characteristics of action potential trains.

5. Stimulation and recording spreading depolarization (SD) in acute brain slices

SD threshold was determined by using localized microinjections of KCl (Seidel and Shuttleworth 2011). A conventional whole-cell patch electrode (tip resistance 3-5 MΩ) was placed 50 μm below the slice surface in stratum radiatum, and microinjections of KCl (1 M) were triggered by brief (10-200 ms) pressure pulses delivered by a PicoPump (SYS-PV830, World Precision Instruments). In a separate set of experiments, SD was induced by inhibition of Na^+/K^+-ATPase activity by superfusion of the slice with ouabain (100 μM).

SD was characterized as a sharp drop in DC potential, as measured with an extracellular recording electrode placed in stratum radiatum (45 μm below the slice surface, ~300 μm from the KCl ejection electrode). Recording electrodes were identical to KCl ejection electrodes, but back-filled with ACSF. Signals were amplified (Neurodata IR-283), digitized (Digitata 1322A, Axon Instruments, Union City, CA) and analyzed using Axoscope software (v 8.1, Axon Instruments).

The propagation of high K^+-SD across the CA1 was monitored from optical signals, generated from epifluorescence excitation at 450 nm (exposure time, 150 ms), and collecting emission 535±25 nm using a monochromator-based imaging system (Till Photonics) with a cooled interline transfer CCD camera (IMAGO, Till Photonics). Imaging at this wavelength produces a mixed signal, including mitochondrial redox potential and swelling signals during the slow progression of SD events. Initial autofluorescence increases provided an indirect measure of initial depolarization and mitochondrial activation (flavoprotein associated), and were used to estimate the degree of tissue activation following KCl

application. The spread of large, delayed fluorescence decreases provided a measure of swelling associated with spreading SD events. Studies of ouabain-SD did not require assessment of initial mitochondrial redox changes. Therefore, ouabain-SD propagation was tracked using changes in light transmittance (>575 nm) as previously described (Andrew et al. 1999) with low-power (4X) observation of both the neocortex and hippocampus.

6. K^+ measurements in vitro

K^+ sensitive electrodes were pulled from theta glass (BT150-10, Sutter Instrument, Novato CA) and the tip broken to a final diameter of 3-6 μm. The reference barrel was back-filled with 150 mM NaCl. The K^+ sensitive barrel was silanized (using sigma coat), tip-filled with 0.5-1 μl potassium ionophore I- cocktail B Selectophore (Sigma), and backfilled with 0.5 M KCl. Voltage responses from each barrels were independently collected with a Multiclamp 700A amplifier and analyzed with pClamp9.2 software (Molecular Devices). Electrodes were inserted in to the striatum radiatum of CA1, ~100 μm from the slice surface. Experiments were conducted after establishment of stable baseline (~20 min after electrode insertion). In every slice, extracellular K^+ responses associated with synaptic stimulation and ouabain-SD were analyzed in a repetitive manner. Slices were first challenged with trains of Schaffer collateral stimulation using a concentric bipolar electrode placed >100 μm from the recording site. Input-output curves were generated in each experiments based on fEPSP detected by the reference barrel. Preparation from CNTF animal tended to show small fEPSP (see Figure 4) and, in order to assure accurate measurement, slices with the maximum responses <1.2 mV were discarded. A series of synaptic responses were evoked at 20 Hz for 10 s using 1) 70% maximum intensities and 2) the stimulus intensities to generate 1 mV fEPSP. Slices were allowed to recover at least 10 min after each experiment. The recovery phase of individual evoked K^+ transients were well fit with double exponential decay plots, and time constants reported for the initial decay phase (Sigmaplot 10.0 software). After recovery from the K^+ clearance tests, slices were challenged with 100 μM ouabain (as described above) to test SD threshold. The K^+ sensitivity of electrodes were tested following these three experiments in every slice, based on calibration curves generated by standard solutions (3, 10 and 30 mM KCl, cation concentration adjusted to 150 mM by NaCl) fitted with Nicolsky's equation.

7. Astrocyte coupling in hippocampal slices

Acute transverse hippocampal slices (300 μm) were prepared as previously described (Pannasch et al. 2012) from *12 weeks* old C57BL6 mice injected with *lenti*-LacZ (n=3) or *lenti*-CNTF (n=3) and were maintained at room temperature in a storage chamber that was perfused with ACSF containing (in mM): 119 NaCl, 2.5 KCl, 2.5 $CaCl_2$, 1.3 $MgSO_4$, 1 NaH_2PO_4, 26.2 $NaHCO_3$ and 11 glucose, saturated with 95% O_2 and 5% CO_2, for at least one hour prior to recording. Slices were transferred to a submerged recording chamber mounted on an Olympus BX51WI microscope equipped for infra red-differential interference (IR-DIC) microscopy and were perfused with ACSF at a rate of 1.5 ml/min at room temperature. Cells in the *stratum radiatum* were identified as astrocytes based on morphological and electrophysiological properties (Rouach et al. 2008). Somatic whole-cell recordings were obtained using 5-10 MΩ glass pipettes filled with, in mM: 105 K-gluconate, 30 KCl, 10 HEPES, 10 phosphocreatine, 4 ATP-Mg, 0.3 GTP-Tris, 0.3 EGTA (pH 7.4, 280

mOsm). For intercellular coupling experiments, the internal solution contained biocytin (2 mg/ml), which diffused passively in astrocytes during 20 min in current-clamp mode. Immediately after recording slices were fixed with 4% paraformaldehyde in PBS for 12 h at 4°C. Biocytin was localized by incubating slices in TRITC-conjugated streptavidin (Invitrogen, Carlsbad CA). After several washes, slices were mounted in Fluoromount (Southern Biotechnology) and examined with a confocal laser-scanning microscope (Leica TBCS SP2). Stacks of consecutive confocal images taken at 0.5 μm intervals were acquired using a helium/neon laser at 543 nm and Z projections were reconstructed using Leica Confocal Software. Manual cell counting was performed with Image J software.

8. Reagents and Solutions

Except where noted, all drugs and salts were obtained from Sigma Chemical Co. (St Louis, MO). Phosphate buffered saline (PBS) was from Invitrogen (Carlsbad, CA, USA). Antibodies were diluted in PBS supplemented with 0.2% Triton X-100 (PBST) and including 3% normal goat serum. 8-Cyclopentyl-1,3-dipropylxanthine (DPCPX, 200 μm stock) was dissolved in DMSO and stored at −20°C until use. Ouabain was dissolved in ACSF (100 μm). Neurobiotin (1%) was dissolved in normal intracellular solution containing the following, in mM: 135 K-gluconate, 8 NaCl, 1$MgCl_2$, 10 HEPES, 2 Mg^{2+}-ATP.

9. Statistical Analysis

Significant differences between group data were evaluated using independent Student's t-tests or one-way ANOVA (F-tests). Tukey's range test was used for post hoc analysis in which the effects of multiple treatments were compared against each other. A value of $p<.05$ was considered significant in all cases. Numbers in the study refer to the number of slices, with a maximum of three slices from an individual animal used for each experimental protocol.

RESULTS

CNTF induces long-term activation of hippocampal astrocytes

Intrahippocampal stereotaxic injection of the lentiviral vector encoding LacZ resulted in effective transduction of hippocampal neurons as observed with β-galactosidase immunostaining (Figure 1A). Significant β-galacotosidase expression was observed in nerve cell bodies in CA1 and CA2 subregions, the dentate granule cells and hilus, but was not observed in brain regions outside the hippocampus, including the neocortex. A similar distribution of β-galactosidase labeling was observed throughout the rostro-caudal axis of the hippocampus in two animals examined (data not shown).

Injection of CNTF-expressing lentiviral vector resulted in strong activation of hippocampal astrocytes, as demonstrated by increases in GFAP. Individual astrocytes showed a marked increase in thickness of the main GFAP-positive immunoreactive processes, when compared with LacZ injected controls, and naïve (non-injected) animals (Figure 1B). This was assessed in thick brain slices prepared for electrophysiological analysis (see Methods) and activation was verified throughout the course of the study in preparations from each animal used for electrophysiological recording. GFAP immunoreactivity was significantly increased

in CNTF preparations compared with LacZ and non-injected controls (Figure 1C, n= 8, 8, 7 respectively). Animals used for quantitative analysis were 8-12 weeks post-injection and additional studies showed that CNTF preparations 16 weeks post-injection continued to show elevated GFAP expression. We also quantified the average density of astrocytes (Figure 1C), and found no significant difference between CNTF, LacZ, and non-injected control preparations (measured in a volume of 300×300×20 μm). To further confirm astrocyte activation, GFAP mRNA levels were quantified using RT-qPCR. There was an almost ten-fold increase in GFAP mRNA expression in CNTF hippocampus compared with LacZ controls (Figure 1D). Together, these results suggest that CNTF expression resulted in localized, long-term activation of astrocytes.

As a control, we examined neuronal distribution, and found that CNTF expression did not lead to changes in the density or structure in the CA1. Estimates of CA1 pyramidal cell number were made from DAPI counts of nuclei in stratum pyramidale in confocal stacks (10 μm thickness) and showed no significant difference between CNTF and LacZ controls (9160±331 cells/mm^2 and 8920±838 cells/mm^2 respectively, n=5, F(1,9)=.071, p=.80, One-way ANOVA). The density of apical dendritic projections (as calculated from MAP-2 immunoreactive processes in 20×150×10 μm confocal stacks centered 200 μm from stratum pyramidale) also showed no significant differences between CNTF and LacZ preparations (29.6±2.7 vs. 35.0±8.6 dendrites/stack respectively, n=5, F(1,9)=.358, p=.566, One-way ANOVA).

Increased K^+-induced SD threshold in CNTF preparations

SD was reliably triggered by localized microinjections of KCl (1 M) in all LacZ preparations. Localized KCl pulses of progressively increasing duration were used to determine the threshold of these all-or-none events, and revealed a threshold between 30-100 ms in LacZ preparations (n=18). SDs were recorded electrically as a sharp negative voltage shift in extracellular DC potential at a recording site ~300 μm from the KCl injection site (Figure 2A). The propagation of SD in LacZ preparations was readily monitored by large optical signal decreases that spread across the CA1 region with an average speed of was 3.85±0.21 mm/min (Figure 2B). For LacZ preparations, the propagation of SD was visually tracked at least as far as the edge of the field of view (~1300 μm) in 7/11 preparations, and all SDs generated by KCl microinjection were fully recoverable and could be evoked repetitively at 10 min intervals.

In contrast, KCl injections never resulted in SD in CNTF preparations. Negative DC shifts, indicative of SD, were never observed over the range of stimuli effective in LacZ tissues (Figures 2C, E), and even when the stimulus duration was increased (500 ms), no propagating event was observed optically or electrically (Figure 2C and D). The lack of spreading events was confirmed by analysis of the delayed optical signal decreases that occurred post-KCl ejection. These relatively sustained optical signal decreases are a consequence of the tissue swelling that accompanies tissue depolarization, and were found to spread no further within 10 s of the KCl stimulus (Figure 2D and F). Therefore, these optical signal decreases likely represent the consequences of passive KCl spread from the stimulating electrode and not SD initiation.

Comparison of the initial components of autofluorescence transients also suggested that the lack of high K^+-SD in CNTF preparations was not due to differences in effective depolarization of the tissue surrounding the stimulating electrode. Initial autofluorescence (E_x 450 nm) increases following KCl ejection were matched by NAD(P)H autofluorescence (E_x 360 nm) decreases, and therefore provide an indication of mitochondrial redox potential changes in stimulated tissue (Shuttleworth et al. 2003). Consistent with similar initial activation, we found no significant difference in initial autofluorescence transients between LacZ and CNTF preparations (7.2±0.6% and 7.9±1.1% respectively at 100 ms KCl pulse, p=.49).

CNTF astrocyte activation is associated with enhanced extracellular K^+ clearance

Astrocyte coupling was compared in LacZ and CNTF preparations since previous work has shown that disruption of gap junctional networks can both increase and decrease SD propagation (Nedergaard et al. 1995; Theis et al. 2003). Dye coupling in astrocyte networks was determined by injection of biocytin into single astrocytes and counting the number of coupled cells (Figure 3A). No significant difference in the degree of coupling was observed between LacZ (n=8) and CNTF (n=9) tissues (Figure 3B, 27.9±4.4 vs. 26.0±3.5 coupled cells, respectively, t(15)=.335, p=.74, independent t-test).

Because glutamate receptor activation can contribute to the spread of SD, we examined whether glutamate-mediated synaptic transmission was modified in CNTF tissues. Excitatory postsynaptic potentials (fEPSPs) recorded in area CA1 were significantly decreased in CNTF preparations, throughout the range of stimulus intensities tested (Figure 4A, LacZ n=7, CNTF n=6). Normalization of fEPSPs to maximal responses in each preparation showed that there was no difference in the stimulus required for half-maximal responses (LacZ: 146±6 μA and CNTF: 149±4 μA), implying a significant difference in efficacy, rather than sensitivity.

We examined whether intrinsic membrane properties of CA1 neurons (assessed from intracellular recordings) were significantly different between the CNTF and LacZ groups. When tested at a resting membrane potential of −65 mV, input resistances were almost identical (87.5±10.8 and 92.7±10.8 MΩ for LacZ and CNTF, respectively; n=10 and 12, p=.74, independent t-test) and depolarizing current pulses (100-500 pA) produced very similar trains of action potentials (no significant difference in number of events, p=.24, independent t-test) and degrees of spike frequency adaptation during long stimuli (Figure 4B).

We next studied extracellular K^+ homeostasis in LacZ and CNTF slices preparations since accumulation of extracellular K^+ is critical for SD initiation. Using RT-qPCR, we assessed mRNA levels of three major transporters involved in K^+ uptake by astrocytes (Larsen et al. 2014). mRNA levels of the α2 subunit of the Na^+/K^+-ATPase was significantly increased (by 46%, p=.032) while levels of $K_{ir}4.1$ and NKCC1 were not different between CNTF and LacZ samples (Figure 3C, LacZ n=6, CNTF n=6). In a set of slice studies, K^+ accumulation and clearance rates were evaluated using two stimulation intensities (recording configuration illustrated in Figure 4C); 1) 70% maximum stimulation intensity and 2) intensity adjusted to generate a 1 mV fEPSP. As described above, with 70% maximum intensity, mean fEPSP amplitudes were significantly smaller in CNTF preparations (Figure 4A) and resulted in

smaller peak K^+ accumulation when compared with LacZ controls (4.36±0.13 mM and 5.34±0.28 mM, respectively, t(22)=3.148, p=.0047, independent t-test)). In order to more precisely compare K^+ clearance rates, we adjusted the stimulus intensity for each experiment to generate a 1 mV fEPSP. With the stimulus intensity normalized, peak K^+ concentrations were no longer significantly different between LacZ and CNTF preparations (4.75±0.72 mM and 4.27±0.44 mM respectively, t(22)=1.961, p=.063, independent t-test). However, the decay kinetics of the K^+ responses were still significantly faster in the CNTF slices when compared with LacZ controls (Figure 4D-F). These results suggest that CNTF preparations had more rapid clearance of extracellular K^+ post-stimulus compared to LacZ controls which could be the result of increased Na^+/K^+-ATPase α2 expression.

Involvement of the Na^+/K^+-ATPase pump in the reduced susceptibility to SD of CNTF tissues

To investigate the role of the Na^+/K^+-ATPase pump in the resistance of CNTF tissue to SD, we tested the effects of extended ouabain (100 μM) exposures. Ouabain inhibits Na^+/K^+-ATPase activity and is known to be an effective stimulus to induce SD in brain slices (Basarsky et al. 1998; Dietz et al. 2008). In LacZ preparations, SDs were induced in all preparations 7.32±0.14 min after ouabain reached the bath and propagated at a rate of 4.43±0.27 mm/min (Figure 5A-B, n=12). At 100 μM concentrations, SD was also generated in all CNTF preparations (n=12). However, the time to SD onset was significantly longer (Figure 5A and 5C) and the mean propagation rate significantly slower (Figure 5B). In addition, there was a trend towards a reduction in the final peak concentration of extracellular K^+ in CNTF preparations when compared with LacZ controls (Figure 5C-D). As an internal control, we simultaneously measured SD in the adjacent neocortex (using low power intrinsic optical imaging for these studies, see Methods). Ouabain-SD propagation rates in neocortex were not significantly different between CNTF and LacZ slices (3.62±0.60 mm/min and 3.78±0.69 mm/min respectively, n=6 and 5, t(9)=0.4198, p=.69, independent t-test), consistent with the hypothesis that differences in ouabain-induced SD were related to CNTF-activated astrocytes, which were confined to the hippocampus with the localized injections in the current study.

DISCUSSION

The main conclusions from this study are 1) that an *in vivo* CNTF expression model can be used to successfully produce long-term activation of astrocytes in the hippocampus 2) the threshold for SD is substantially elevated in tissues with activated astrocytes, and 3) this increase in SD threshold may be the result of changes in K^+ homeostasis by astrocytes. These findings are consistent with the hypothesis that astrocyte activation could limit the incidence of SD and thus provide neuroprotection in some neurological or neurodegenerative disorders.

CNTF model for astrocyte activation

In mature astrocytes, CNTF triggers a cascade of intracellular events involving the JAK-STAT pathway that leads to the generation of an activated phenotype (Bonni et al. 1997; Hudgins and Levison 1998). Under normal physiological conditions, CNTF is expressed

predominantly by astrocytes in the mature brain, with little (if any) neuronal expression (Dallner et al. 2002). Our experimental model involves transduction of neurons with a lentivirus and constitutive release of CNTF into the extracellular space (up to 1 ng/mg protein, see (de Almeida et al. 2001)), and our results demonstrate robust and sustained activation of murine hippocampal astrocytes, as has been described previously following injection of the same lentiviral construct into rat striatum (Beurrier et al. 2010; Escartin et al. 2006; Escartin et al. 2007). Direct injection of CNTF has also recently been reported to produce hippocampal astrocyte activation *in vivo* that is sustained for at least 3 weeks (Bechstein et al. 2012). Even if we cannot rule out the possibility that CNTF exposure could have significant direct effects on neuronal function, the observation that CNTF increased levels of STAT3 and nuclear localization of STAT3 specifically in GFAP-positive astrocytes and not into neurons (Escartin et al, 2006; Bechstein et al., 2012), suggest that astrocytes are the main cellular targets of CNTF. Because hippocampal slices are widely used for electrophysiological studies, *in vivo* lentiviral injections allow for constitutive, long term expression of CNTF which could be useful to assess functional consequences of astrocyte activation on many aspects of neuronal-glial interactions, in addition to the question of SD susceptibility.

Consequences of prolonged CNTF exposure on astrocyte and synaptic function

Increased GFAP immunolabeling is a well-established anatomical hallmark of astrocyte activation following a range of stimuli (Kalman 2004; Pekny and Nilsson 2005), yet the associated functional changes are not well characterized. Recent work has evaluated a range of functional consequences linked to astrocytes activation by CNTF. Activation is accompanied by a stable shift in metabolic substrate utilization to a more oxidative phenotype (Escartin et al. 2007) suggesting that CNTF-activated astrocytes may have a strong protective potential to face metabolic insults (Escartin et al. 2007). Furthermore, CNTF overexpression produced a redistribution of GLAST and GLT-1 into raft functional membrane microdomains, which are important for glutamate uptake (Escartin et al. 2006).

A reduction in overall astrocytic intercellular communication in mice lacking connexin 43 was found to be associated with an increase in the velocity of hippocampal SD (Theis et al., 2003) and we previously found an increased expression of connexin 43 by CNTF exposure in rat striatum (Escartin et al. 2006). However, we did not find significant differences in astrocyte coupling in the present study, suggesting that changes in gap junctional communication of astrocyte networks are not major contributors to effects of CNTF on SD threshold.

Interestingly, we found a significant increase in mRNA levels of the α2 subunit of the Na^+/K^+-ATPase, which is found primarily in glial cells in the adult brain (Cholet et al. 2002). In astrocytes, the Na^+ required for maintained Na^+/K^+-ATPase activity can be provided by co-transport mechanisms (Rose and Ransom 1996) and it has been suggested that Na^+/K^+-ATPase activity is a predominant mechanism of K^+ clearance following SD (Lian and Stringer 2004). Our results from 70% maximal synaptic stimulation showed a significant decrease in both the amplitude and decay rate of K^+ transients in CNTF tissues compared with LacZ controls. Recent work has shown that that spatial buffering by K_{ir} channels

occurs during local extracellular K^+ increases, while Na^+/K^+-ATPase pump activity (particularly the astrocytic α2β2 isoform) is important for post-stimulus clearance of extracellular K^+ (Larsen et al. 2014) (see also (Ransom et al. 2000)). This raises the possibility that both K_{ir}-mediated spatial buffering and Na^+/K^+-ATPase post-stimulus clearance could be increased in CNTF tissues. However, we no longer observed a reduction in the amplitude of K^+ transients when the stimulus intensity was normalized to produce a 1 mV fEPSP, suggesting K_{ir} spatial buffering may not be involved. The decrease in the decay rate post-stimulus was still observed when the stimulus was normalized to produce a 1 mV fEPSP. This finding, along with our RT-qPCR data, lead us to suggest that increased Na^+/K^+-ATPase pump activity in CNTF-activated astrocytes could underlie the increased K^+ clearance observed in these tissues. We cannot completely exclude the possibility of changes to other K^+ channels contributing to the increased K^+ clearance observed in CNTF tissues since they were not directly tested in these studies. However, since it is widely accepted in the field that astrocytes are the predominant cell type to clear extracellular K^+, we suggest that any changes observed in the K^+ signal, when the neuronal response is standardized, are likely due to phenotypic changes to astrocytes.

We found a significant decrease in synaptic efficacy in studies of stimulation of glutamatergic inputs from Shaffer collateral fibers to CA1 pyramidal neurons. One of the many ways in which astrocytes have been suggested to modulate synaptic activity is by the release of adenosine at the synapse to decrease presynaptic release of glutamate (Dunwiddie and Masino 2001; Pascual et al. 2005). However, addition of the A1 receptor antagonist, DPCPX, did not restore CNTF fEPSPs to similar levels as LacZ preparations (data not shown). The mechanism(s) underlying changes in synaptic potential amplitude are not yet known, but possibilities include morphological changes of astroglial processes inducing modulation in glutamate transport at synapses (Pannasch et al. 2014), as well as possible adaptive changes in postsynaptic glutamate receptor sensitivity.

Changes in SD threshold

SD threshold can be determined by progressively increasing the intensity of electrical or KCl stimulation to the brain surface *in vivo* or brain slice. In our studies, we characterized the threshold for SD by using graded, localized 1 M KCl microinjections, delivered by pressure pulses of increasing duration from a conventional patch electrode. Rapid and localized extracellular K^+ elevations are expected to depolarize a population of cells, and subsequent glutamate and/or K^+ release from these cells is thought to underlie the feed-forward propagation of the SD event (Kager et al. 2000; Somjen 2001). Once initiated, SD progressed slowly (~3-5 mm/min) from the injection site. While SD threshold could be readily determined in each LacZ control slice (generally between 30-100 ms pulse duration), SD could not be induced even with prolonged KCl microinjection in CNTF preparations. This striking difference was not due to differences in the KCl microinjection, since the same delivery electrodes were utilized for paired CNTF and LacZ studies on individual recording days, and autofluorescence studies of mitochondrial activation indicated similar degrees of slice activation at the KCl ejection site (data not shown).

Subsequent experiments with bath application of 100 μM ouabain revealed that CNTF tissues do retain the ability to generate SD, albeit with a significantly longer latency to onset and significantly slower propagation rate than was observed in LacZ controls. By confirming that CNTF tissues retain appropriate structural and functional properties required for SD, this observation provides a useful control for the KCl studies. In addition, the fact that ouabain triggers SD by a very different mechanism (inhibition of the Na^+/K^+-ATPase) may provide insight into possible mechanisms by which CNTF limits SD. The ouabain concentration (100 μM) used for these experiments has previously been shown to reliably generate SD in brain slices (Balestrino et al. 1999; Basarsky et al. 1998; Dietz et al. 2008; Haglund and Schwartzkroin 1990), and is expected to completely inhibit Na^+/K^+-ATPase pumps containing α2 and α3 isoforms ($K_{0.5}$= 64 and 23 nM, respectively) and at least partially inhibiting those containing α1 isoforms ($K_{0.5}$=91 μM) (Blanco et al. 1993; Pellerin and Magistretti 1997). The α1 isoform can be found in both neurons and astrocytes, while the α2 isoform is expressed mainly in astrocytes and the α3 isoform is found predominately in neurons (Cholet et al. 2002; McGrail et al. 1991; Watts et al. 1991). Lower concentrations of ouabain were tested, but 100 μM was required to reliably induce SD in all CNTF slices (data not shown). Inhibition of the Na^+/K^+-ATPase on neurons will lead to rapid depolarization and release of K^+ and glutamate into the extracellular space. The main difference between the two stimuli is that ouabain will also lead to a significant impairment in both Na^+-dependent glutamate and K^+ uptake by astrocytes as a consequence of Na^+/K^+-ATPase inhibition. K^+ recordings and qPCR measurements from the current study suggest that increase K^+ uptake by astrocyte could be sufficient to prevent the propagation of high K^+-SD and could explain the increased latency and slower propagation of ouabain-SD.

Morphological alterations of astrocytes by CNTF could also change the volume of the extracellular space (ECS) (Sykova 2001) and the diffusion properties of K^+, contributing to altered SD induction threshold in CNTF animals. Exploration of the ECS properties in our experimental model of CNTF-induced astrocyte activation would be of interest to address this issue. Finally, it cannot be ruled out that the significant decrease in SD susceptibility observed in CNTF-injected tissues is the result of direct changes in neuronal function in addition to the effects on astrocytes, even if the JAK-STAT pathway, the major signaling pathway activated by CNTF overexpression, was previously shown to be selectively activated in astrocytes (Escartin et al. 2006).

Activation of astrocytes by SD and ischemia

A number of studies have described astrocyte activation following SD, as demonstrated by increases in GFAP immunolabeling in the affected tissue (Kraig et al. 1991; Wiggins et al. 2003). This association between SD and astrocyte activation has been demonstrated most clearly in studies of repetitive application of K^+ in otherwise healthy brain. Activation occurred within 6 hours of induced SD events and persisted for at least one week post-SD (Kraig et al. 1991; Wiggins et al. 2003). There have been few studies of the consequences of astrocyte activation following SD, but it is noteworthy that a recent report described a progressive increase in SD threshold when rats are repetitively challenged by SD, and this was associated with astrocyte activation (Sukhotinsky et al. 2011). Our results support the

possibility that astrocyte activation itself could underlie the increased SD threshold, when animals are subjected to repetitive SD *in vivo*.

Recent work has provided increasing support for the hypothesis that repetitive SD events are common following animal and human stroke, and that deleterious consequences of SD can contribute to the enlargement of acute brain injures (Lauritzen et al., 2011, Dreier et al., 2011). It is not yet known whether SD events associated with ischemia contribute to the well-described activation of astrocytes in peri-infarct regions in animal models of stroke (Chen et al. 1993; Li et al. 1995) or in postmortem tissues from human stroke patients (Zhao et al. 2006). However our observations of greatly elevated SD threshold in tissues with CNTF activated astrocytes suggest that peri-infarct activated astrocytes could serve to limit the spread of SD into healthy brain tissue following stroke. Finally, it is possible that the mechanism underlying the protective effects of these activated astrocytes is increased K^+ uptake by the Na^+/K^+-ATPase on astrocytes. Regardless, these studies do provide evidence consistent with an important supportive role for astrocytes, and suggest that maintaining normal astrocytic function in compromised tissue may be valuable for preventing repetitive depolarizing events which contribute to the expansion of brain injury.

ACKNOWLEDGEMENTS

Supported by NIH grant NS051288 (C.W.S), Commissariat à l'Energie Atomique (CEA; http://www.cea.fr/), Centre National de la Recherche Scientifique (CNRS; http://www.cnrs.fr/) (GB), and Institut National de la Sante et de la Recherche Medicale (INSERM) (NR).

REFERENCES

Andrew RD, Jarvis CR, Obeidat AS. Potential sources of intrinsic optical signals imaged in live brain slices. Methods. 1999; 18(2):185–96. 179. [PubMed: 10356350]

Balestrino M, Young J, Aitken P. Block of (Na+,K+)ATPase with ouabain induces spreading depression-like depolarization in hippocampal slices. Brain Res. 1999; 838(1-2):37–44. [PubMed: 10446314]

Basarsky TA, Duffy SN, Andrew RD, MacVicar BA. Imaging spreading depression and associated intracellular calcium waves in brain slices. J Neurosci. 1998; 18(18):7189–99. [PubMed: 9736642]

Bechstein M, Haussler U, Neef M, Hofmann HD, Kirsch M, Haas CA. CNTF-mediated preactivation of astrocytes attenuates neuronal damage and epileptiform activity in experimental epilepsy. Exp Neurol. 2012; 236(1):141–50. [PubMed: 22542945]

Beurrier C, Faideau M, Bennouar KE, Escartin C, Kerkerian-Le Goff L, Bonvento G, Gubellini P. Ciliary neurotrophic factor protects striatal neurons against excitotoxicity by enhancing glial glutamate uptake. PLoS One. 2010; 5(1):e8550. [PubMed: 20062544]

Blanco G, Xie ZJ, Mercer RW. Functional expression of the alpha 2 and alpha 3 isoforms of the Na,K-ATPase in baculovirus-infected insect cells. Proc Natl Acad Sci U S A. 1993; 90(5):1824–8. [PubMed: 8383329]

Bonni A, Sun Y, Nadal-Vicens M, Bhatt A, Frank DA, Rozovsky I, Stahl N, Yancopoulos GD, Greenberg ME. Regulation of gliogenesis in the central nervous system by the JAK-STAT signaling pathway. Science. 1997; 278(5337):477–83. [PubMed: 9334309]

Canals S, Larrosa B, Pintor J, Mena MA, Herreras O. Metabolic challenge to glia activates an adenosine-mediated safety mechanism that promotes neuronal survival by delaying the onset of spreading depression waves. J Cereb Blood Flow Metab. 2008

Charles A, Brennan K. Cortical spreading depression-new insights and persistent questions. Cephalalgia. 2009; 29(10):1115–24. [PubMed: 19735537]

Chen H, Chopp M, Schultz L, Bodzin G, Garcia JH. Sequential neuronal and astrocytic changes after transient middle cerebral artery occlusion in the rat. J Neurol Sci. 1993; 118(2):109–6. [PubMed: 8229058]

Cholet N, Pellerin L, Magistretti PJ, Hamel E. Similar perisynaptic glial localization for the Na+,K+-ATPase alpha 2 subunit and the glutamate transporters GLAST and GLT-1 in the rat somatosensory cortex. Cereb Cortex. 2002; 12(5):515–25. [PubMed: 11950769]

Dallner C, Woods AG, Deller T, Kirsch M, Hofmann HD. CNTF and CNTF receptor alpha are constitutively expressed by astrocytes in the mouse brain. Glia. 2002; 37(4):374–8. [PubMed: 11870876]

de Almeida LP, Zala D, Aebischer P, Deglon N. Neuroprotective effect of a CNTF-expressing lentiviral vector in the quinolinic acid rat model of Huntington's disease. Neurobiol Dis. 2001; 8(3):433–46. [PubMed: 11442352]

Dietz RM, Weiss JH, Shuttleworth CW. Zn^{2+} influx is critical for some forms of spreading depression in brain slices. J Neurosci. 2008; 28(32):8014–24. [PubMed: 18685026]

Dohmen C, Sakowitz OW, Fabricius M, Bosche B, Reithmeier T, Ernestus RI, Brinker G, Dreier JP, Woitzik J, Strong AJ. Spreading depolarizations occur in human ischemic stroke with high incidence. Ann Neurol. 2008; 63(6):720–8. others. [PubMed: 18496842]

Dreier JP. The role of spreading depression, spreading depolarization and spreading ischemia in neurological disease. Nat Med. 2011; 17(4):439–47. [PubMed: 21475241]

Dunwiddie TV, Masino SA. The role and regulation of adenosine in the central nervous system. Annu Rev Neurosci. 2001; 24:31–55. [PubMed: 11283304]

Escartin C, Bonvento G. Targeted activation of astrocytes: a potential neuroprotective strategy. Mol Neurobiol. 2008; 38(3):231–41. [PubMed: 18931960]

Escartin C, Brouillet E, Gubellini P, Trioulier Y, Jacquard C, Smadja C, Knott GW, Kerkerian-Le Goff L, Deglon N, Hantraye P. Ciliary neurotrophic factor activates astrocytes, redistributes their glutamate transporters GLAST and GLT-1 to raft microdomains, and improves glutamate handling in vivo. J Neurosci. 2006; 26(22):5978–89. others. [PubMed: 16738240]

Escartin C, Pierre K, Colin A, Brouillet E, Delzescaux T, Guillermier M, Dhenain M, Deglon N, Hantraye P, Pellerin L. Activation of astrocytes by CNTF induces metabolic plasticity and increases resistance to metabolic insults. J Neurosci. 2007; 27(27):7094–104. others. [PubMed: 17611262]

Fabricius M, Fuhr S, Bhatia R, Boutelle M, Hashemi P, Strong AJ, Lauritzen M. Cortical spreading depression and peri-infarct depolarization in acutely injured human cerebral cortex. Brain. 2006; 129(Pt 3):778–90. [PubMed: 16364954]

Haglund MM, Schwartzkroin PA. Role of Na-K pump potassium regulation and IPSPs in seizures and spreading depression in immature rabbit hippocampal slices. J Neurophysiol. 1990; 63(2):225–39. [PubMed: 2313342]

Hartings JA, Rolli ML, Lu XC, Tortella FC. Delayed secondary phase of peri-infarct depolarizations after focal cerebral ischemia: relation to infarct growth and neuroprotection. J Neurosci. 2003; 23(37):11602–10. [PubMed: 14684862]

Hartings JA, Watanabe T, Bullock MR, Okonkwo DO, Fabricius M, Woitzik J, Dreier JP, Puccio A, Shutter LA, Pahl C. Spreading depolarizations have prolonged direct current shifts and are associated with poor outcome in brain trauma. Brain. 2011; 134(Pt 5):1529–40. others. [PubMed: 21478187]

Hoskison MM, Shuttleworth CW. Microtubule disruption, not calpain-dependent loss of MAP2, contributes to enduring NMDA-induced dendritic dysfunction in acute hippocampal slices. Exp Neurol. 2006; 202(2):302–12. [PubMed: 16904106]

Hossmann KA. Periinfarct depolarizations. Cerebrovasc Brain Metab Rev. 1996; 8(3):195–208. [PubMed: 8870974]

Hudgins SN, Levison SW. Ciliary neurotrophic factor stimulates astroglial hypertrophy in vivo and in vitro. Exp Neurol. 1998; 150(2):171–82. [PubMed: 9527886]

Kager H, Wadman WJ, Somjen GG. Simulated seizures and spreading depression in a neuron model incorporating interstitial space and ion concentrations. J Neurophysiol. 2000; 84(1):495–512. [PubMed: 10899222]

Kalman, M. Glial reaction and reactive glia.. In: Hertz, L., editor. Non neuronal cells of the nervous system: function and dysfunction. Elsevier; Amsterdam: 2004. p. 787-835.

Kraig RP, Dong LM, Thisted R, Jaeger CB. Spreading depression increases immunohistochemical staining of glial fibrillary acidic protein. J Neurosci. 1991; 11(7):2187–98. [PubMed: 1906091]

Largo C, Cuevas P, Somjen GG, Martin del Rio R, Herreras O. The effect of depressing glial function in rat brain in situ on ion homeostasis, synaptic transmission, and neuron survival. J Neurosci. 1996; 16(3):1219–29. [PubMed: 8558250]

Largo C, Ibarz JM, Herreras O. Effects of the gliotoxin fluorocitrate on spreading depression and glial membrane potential in rat brain in situ. J Neurophysiol. 1997; 78(1):295–307. [PubMed: 9242281]

Larsen BR, Assentoft M, Cotrina ML, Hua SZ, Nedergaard M, Kaila K, Voipio J, Macaulay N. Contributions of the Na(+) /K(+) -ATPase, NKCC1, and Kir4.1 to hippocampal K(+) clearance and volume responses. Glia. 2014; 62(4):608–22. [PubMed: 24482245]

Lauritzen M, Dreier JP, Fabricius M, Hartings JA, Graf R, Strong AJ. Clinical relevance of cortical spreading depression in neurological disorders: migraine, malignant stroke, subarachnoid and intracranial hemorrhage, and traumatic brain injury. J Cereb Blood Flow Metab. 2011; 31(1):17–35. [PubMed: 21045864]

Leao A. Spreading depression of activity in the cerebral cortex. Journal of Neurophysiology. 1944; 7:359–390.

Leis JA, Bekar LK, Walz W. Potassium homeostasis in the ischemic brain. Glia. 2005; 50(4):407–16. [PubMed: 15846795]

Li Y, Chopp M, Zhang ZG, Zhang RL. Expression of glial fibrillary acidic protein in areas of focal cerebral ischemia accompanies neuronal expression of 72-kDa heat shock protein. J Neurol Sci. 1995; 128(2):134–42. [PubMed: 7738589]

Lian XY, Stringer JL. Astrocytes contribute to regulation of extracellular calcium and potassium in the rat cerebral cortex during spreading depression. Brain Res. 2004; 1012(1-2):177–84. [PubMed: 15158175]

Lin LF, Mismer D, Lile JD, Armes LG, Butler ET 3rd, Vannice JL, Collins F. Purification, cloning, and expression of ciliary neurotrophic factor (CNTF). Science. 1989; 246(4933):1023–5. [PubMed: 2587985]

Livak KJ, Schmittgen TD. Analysis of relative gene expression data using real-time quantitative PCR and the 2(-Delta Delta C(T)) Method. Methods. 2001; 25(4):402–8. [PubMed: 11846609]

McGrail KM, Phillips JM, Sweadner KJ. Immunofluorescent localization of three Na,K-ATPase isozymes in the rat central nervous system: both neurons and glia can express more than one Na,K-ATPase. J Neurosci. 1991; 11(2):381–91. [PubMed: 1846906]

Nedergaard M, Astrup J. Infarct rim: effect of hyperglycemia on direct current potential and [14C]2-deoxyglucose phosphorylation. J Cereb Blood Flow Metab. 1986; 6(5):607–15. [PubMed: 3760045]

Nedergaard M, Cooper AJ, Goldman SA. Gap junctions are required for the propagation of spreading depression. J Neurobiol. 1995; 28(4):433–44. [PubMed: 8592104]

Nedergaard M, Hansen AJ. Spreading depression is not associated with neuronal injury in the normal brain. Brain Res. 1988; 449(1-2):395–8. [PubMed: 3395856]

Pannasch U, Freche D, Dallerac G, Ghezali G, Escartin C, Ezan P, Cohen-Salmon M, Benchenane K, Abudara V, Dufour A. Connexin 30 sets synaptic strength by controlling astroglial synapse invasion. Nat Neurosci. 2014; 17(4):549–58. others. [PubMed: 24584052]

Pannasch U, Sibille J, Rouach N. Dual electrophysiological recordings of synaptically-evoked astroglial and neuronal responses in acute hippocampal slices. J Vis Exp. 2012; (69):e4418. [PubMed: 23222635]

Pascual O, Casper KB, Kubera C, Zhang J, Revilla-Sanchez R, Sul JY, Takano H, Moss SJ, McCarthy K, Haydon PG. Astrocytic purinergic signaling coordinates synaptic networks. Science. 2005; 310(5745):113–6. [PubMed: 16210541]

Pekny M, Nilsson M. Astrocyte activation and reactive gliosis. Glia. 2005; 50(4):427–34. [PubMed: 15846805]

Pellerin L, Magistretti PJ. Glutamate uptake stimulates Na+,K+-ATPase activity in astrocytes via activation of a distinct subunit highly sensitive to ouabain. J Neurochem. 1997; 69(5):2132–7. [PubMed: 9349559]

Ransom CB, Ransom BR, Sontheimer H. Activity-dependent extracellular K+ accumulation in rat optic nerve: the role of glial and axonal Na+ pumps. J Physiol. 2000; 522(Pt 3):427–42. [PubMed: 10713967]

Risher WC, Croom D, Kirov SA. Persistent astroglial swelling accompanies rapid reversible dendritic injury during stroke-induced spreading depolarizations. Glia. 2012; 60(11):1709–20. [PubMed: 22821441]

Rose CR, Ransom BR. Intracellular sodium homeostasis in rat hippocampal astrocytes. J Physiol. 1996; 491(Pt 2):291–305. [PubMed: 8866855]

Rouach N, Koulakoff A, Abudara V, Willecke K, Giaume C. Astroglial metabolic networks sustain hippocampal synaptic transmission. Science. 2008; 322(5907):1551–5. [PubMed: 19056987]

Seidel JL, Shuttleworth CW. Contribution of astrocyte glycogen stores to progression of spreading depression and related events in hippocampal slices. Neuroscience. 2011; 192:295–303. [PubMed: 21600270]

Shuttleworth CW, Brennan AM, Connor JA. NAD(P)H fluorescence imaging of postsynaptic neuronal activation in murine hippocampal slices. J Neurosci. 2003; 23(8):3196–208. [PubMed: 12716927]

Shuttleworth CW, Connor JA. Strain-dependent differences in calcium signaling predict excitotoxicity in murine hippocampal neurons. J Neurosci. 2001; 21(12):4225–36. [PubMed: 11404408]

Somjen GG. Mechanisms of spreading depression and hypoxic spreading depression-like depolarization. Physiol Rev. 2001; 81(3):1065–96. [PubMed: 11427692]

Strong AJ, Smith SE, Whittington DJ, Meldrum BS, Parsons AA, Krupinski J, Hunter AJ, Patel S, Robertson C. Factors influencing the frequency of fluorescence transients as markers of peri-infarct depolarizations in focal cerebral ischemia. Stroke. 2000; 31(1):214–22. [PubMed: 10625740]

Sukhotinsky I, Dilekoz E, Wang Y, Qin T, Eikermann-Haerter K, Waeber C, Ayata C. Chronic daily cortical spreading depressions suppress spreading depression susceptibility. Cephalalgia. 2011

Sykova E. Glial diffusion barriers during aging and pathological states. Prog Brain Res. 2001; 132:339–63. [PubMed: 11545002]

Theis M, Jauch R, Zhuo L, Speidel D, Wallraff A, Doring B, Frisch C, Sohl G, Teubner B, Euwens C. Accelerated hippocampal spreading depression and enhanced locomotory activity in mice with astrocyte-directed inactivation of connexin43. J Neurosci. 2003; 23(3):766–76. others. [PubMed: 12574405]

Watts AG, Sanchez-Watts G, Emanuel JR, Levenson R. Cell-specific expression of mRNAs encoding Na+,K(+)-ATPase alpha- and beta-subunit isoforms within the rat central nervous system. Proc Natl Acad Sci U S A. 1991; 88(16):7425–9. [PubMed: 1651505]

Wiggins AK, Shen PJ, Gundlach AL. Delayed, but prolonged increases in astrocytic clusterin (ApoJ) mRNA expression following acute cortical spreading depression in the rat: evidence for a role of clusterin in ischemic tolerance. Brain Res Mol Brain Res. 2003; 114(1):20–30. [PubMed: 12782389]

Zhao J, Mao Y, Qi J. Expression of cytoskeleton and apoptosis related genes after cerebral infarction. Neurol Res. 2006; 28(1):71–5. [PubMed: 16464366]

MAIN POINTS

We found that constitutive CNTF expression led to long-term activation of astrocytes which significantly elevated spreading depolarization (SD) threshold. This increase in SD threshold may be the result of changes in K^+ homeostasis in CNTF tissues.

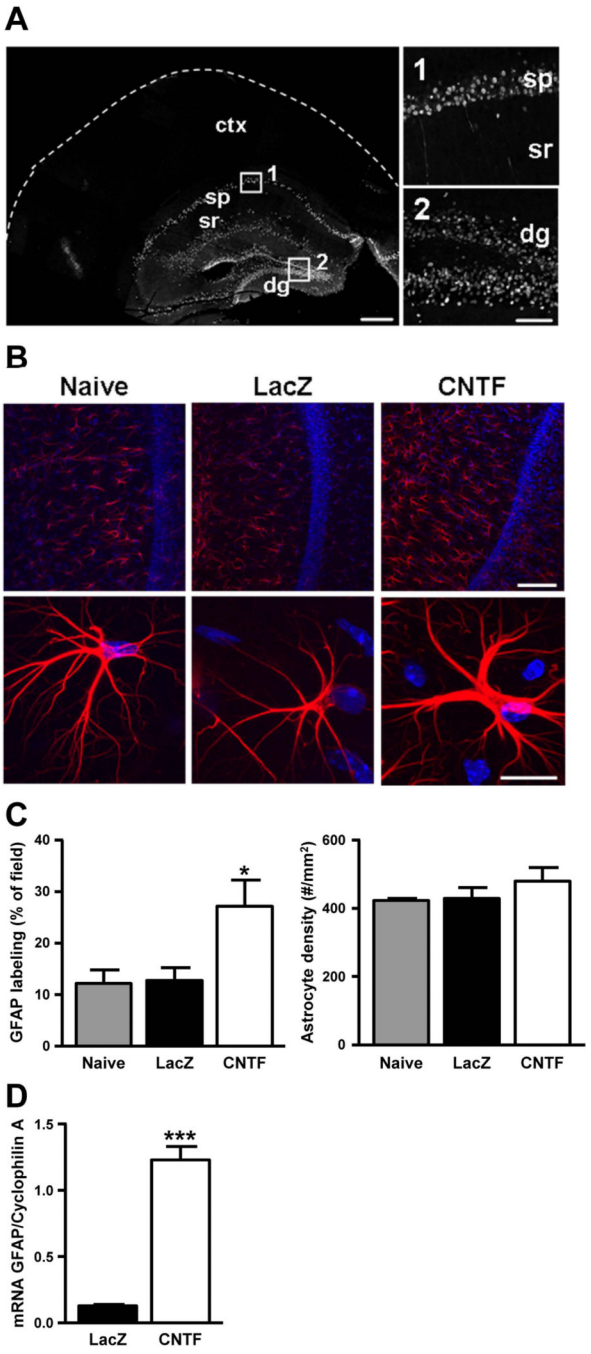

Figure 1. Astrocyte activation within murine hippocampus

A. Representative distribution of β-galactosidase immunohistochemistry demonstrates that intrahippocampal lentivirus injections lead to infection localized within the hippocampus, and high power confocal images of the CA1 and dentate gyrus showing localization to neuronal cell bodies (30 μm cryostat section, scale bar: 1 mm and 100 μm respectively). **B.** GFAP immunohistochemistry: Low power confocal projections (20 μm thick) were used to quantify changes in either total astrocyte number or simply increases in GFAP expression within resident astrocytes in hippocampal slice preparations (250 μm sections) from mice

injected with lenti-CNTF versus lenti-LacZ as well as none injected controls (top panel, n= 8/8/7). Representative high power confocal images (20 μm thick) show increased GFAP within single astrocytes from CNTF hippocampal slices versus LacZ and controls (bottom panel). (GFAP: red, DAPI: blue, Scale bars: top panel 100 μm, bottom panel 50 μm). **C.** Quantification of area expressing GFAP and total astrocyte density. There was a significant increase in GFAP expression in CNTF preparations when compared with both LacZ and non-injected controls ($F(2,22)=5.049$, *p=.017, One-way ANOVA with Tukey's post-hoc test), but no significant difference in total number of astrocytes ($F(2,22)=.968$, p=.40, One-way ANOVA with Tukey's post-hoc test). **D.** RT-qPCR was used to measure GFAP mRNA levels in CNTF and LacZ hippocampal tissue. Cyclophilin A served as a housekeeping gene and was used to normalize the expression levels of the genes of interest. There was a significant increase in GFAP mRNA ($t(10)=10.97$, ***p=.0001, independent t-test) in CNTF tissue compared with LacZ controls.

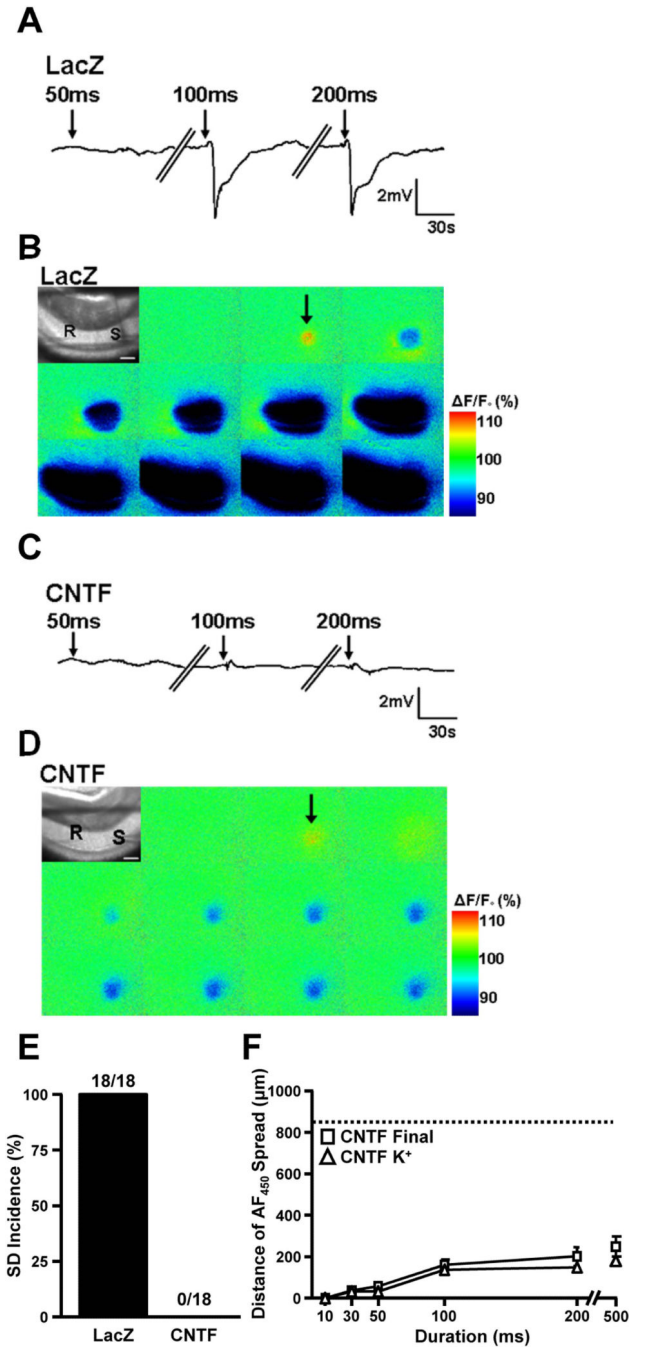

Figure 2. Inhibition of SD in slices with CNTF-activated astrocytes

A. Representative DC recordings from LacZ preparations during 50 ms, 100 ms, and 200 ms KCl microinjections with 10 min intervals between stimuli. Recordings (R) were taken ~300 μm from the KCl injection site (S) as shown in bright field images in top corner of montages (**B**). **B.** Representative montage of 450 nm autofluorescence during the 100 ms KCl microinjection (shown electrically in **A**) from the LacZ preparation which resulted in the propagation of SD across the preparation beyond the field of view (~1300 μm). **C.** Representative DC recording from a CNTF preparation where KCl microinjections up to

200 ms in duration did not result in SD. **D.** Representative 450 nm autofluorescence recording during the 100 ms KCl microinjection from the CNTF preparation where the initial passive depolarization due to the exogenous KCl application occurred, but no propagating SD event. **E.** SD threshold determined with high K^+ microinjections (1 M KCl). In LacZ slices SDs were induced in all preparations by the longest K^+ microinjection (200 ms) (n=18/18). The same stimuli did not generate an SD in any CNTF preparations (n=0/18). **F.** Distance of the final tissue depolarization in CNTF preparations versus the initial passive depolarization due to the spread of exogenous K^+. CNTF preparations showed no significant differences between the passive K^+ depolarization (white triangles) and the final response (white boxes), providing further support for the lack of SD in CNTF preparations (n=12, dashed line represents the average distance of the view frame).

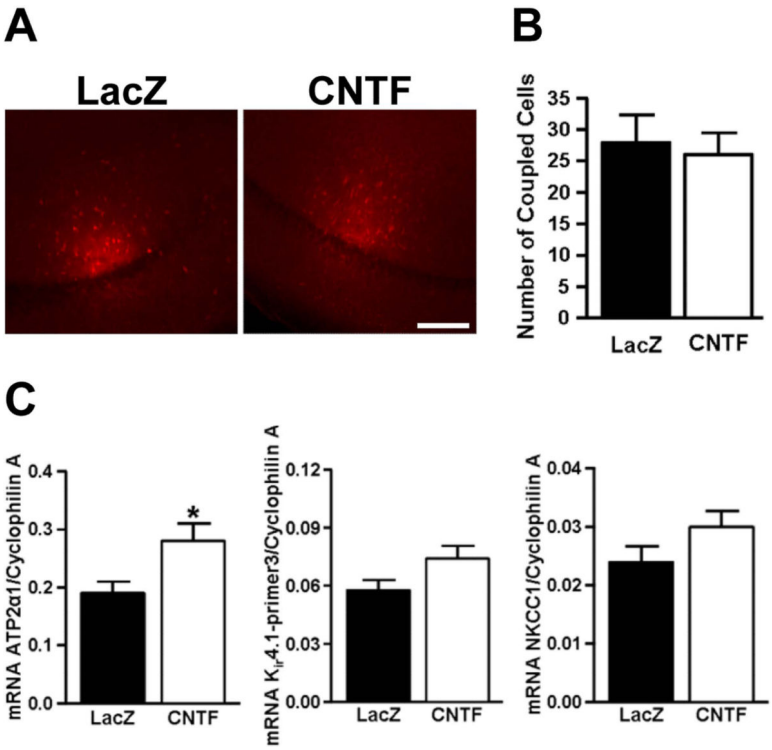

Figure 3. CNTF-activated astrocytes display unchanged gap junctional coupling, but increased mRNA for the α2 subunit of the Na^+/K^+-ATPase

A. Representative low-power images from slice preparations where single astrocytes were loaded with biocytin to assess astrocytic coupling (scale bar: 150 μm). **B.** No significant difference in astrocyte coupling between LacZ and CNTF preparations, as assessed by the number of biocytin positive astrocytes (t(15)=.335, p=.74, independent t-test). **C.** RT-qPCR was used to measure mRNA levels in CNTF and LacZ hippocampal tissue. Cyclophilin A served as a housekeeping gene and was used to normalize the expression levels of the genes of interest. There was a significant increase in ATP-2alpha1 (t(10)=2.496, *p=.032, independent t-test), but no significant difference in $K_{ir}4.1$ (t(10)= 1.922, p=.0835, independent t-test) and NKCC1 (t(10)= 1.571, p=.15) expression in CNTF tissue compared with LacZ controls.

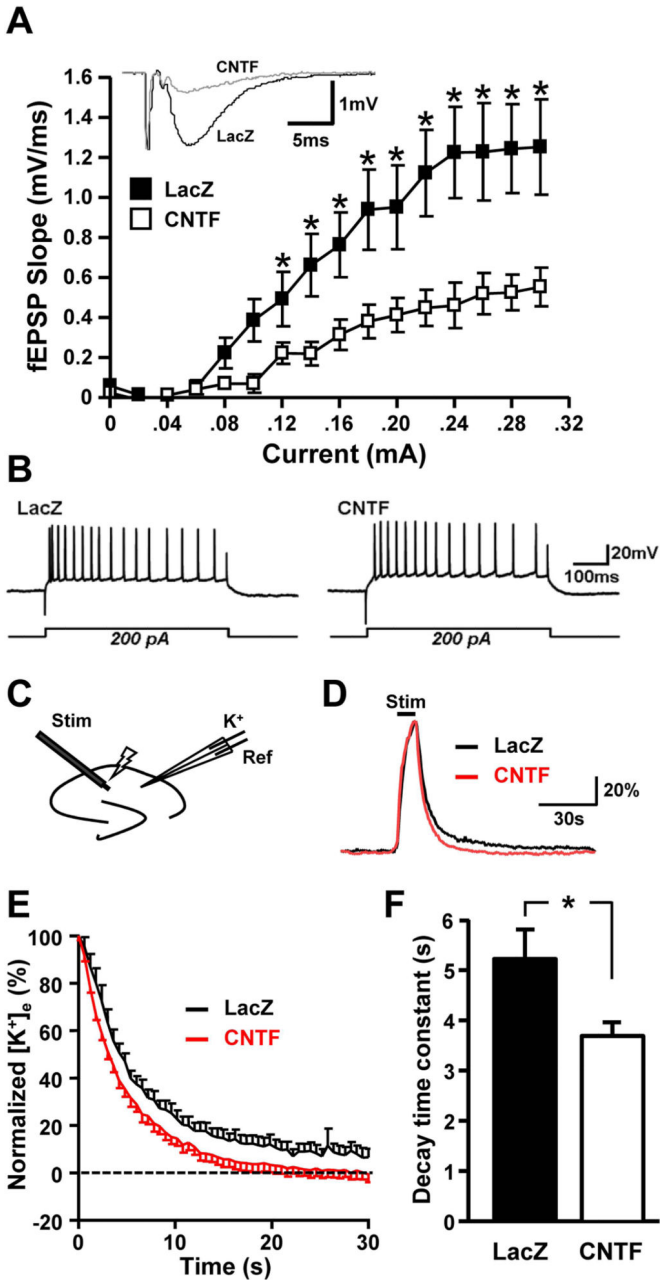

Figure 4. CNTF astrocytes activation results in reduced glutamatergic synaptic efficacy and increased K^+ homeostasis

A. Input-output curves were generated from the slope of fEPSP at increasing currents (0.0-0.3 mA, 0.02 mA interval). There was a significant decrease in the slope of the fEPSPs in CNTF hippocampal slices when compared to LacZs (n=6 and n=7 respectively, $F(2,10)=4.32$, * $p<.05$, One-way ANOVA with Tukey's post-hoc test). Representative fEPSP traces from LacZ (black) and CNTF (grey) preparations are from a stimulus of 0.2 mA. **B.** Intrinsic membrane properties of neurons were also not significantly different between CNTF and LacZ controls. **C.** Extracellular K^+ transients were evoked using electrical stimulation of Schaffer collateral inputs (20 Hz, 10 s), and recorded with double barreled K^+

sensitive microelectrodes placed in stratum radiatum of area CA1. K^+ accumulation and clearance rates were evaluated using two different stimulation intensities; 1) 70% stimulation intensity required to generate just maximal amplitude fEPSPs, and 2) stimulation intensity adjusted to generate matched 1 mV amplitude fEPSP. **D.** Representative individual responses to matched (1 mV fEPSP) stimuli in LacZ (black) and CNTF (red) preparations. Responses are normalized to peak amplitudes. **E.** Decay phase of evoked K^+ transients from populations of experiments illustrated in panel **D**. (mean ± SEM shown, n=12 preparations for each group). **F.** Significantly shorter decay time constants in CNTF preparations. Data were derived from same preparations illustrated in panel **E**, with stimuli matched to generate 1 mV fEPSPs (n=12 for each group, *p=.026, independent t-test).

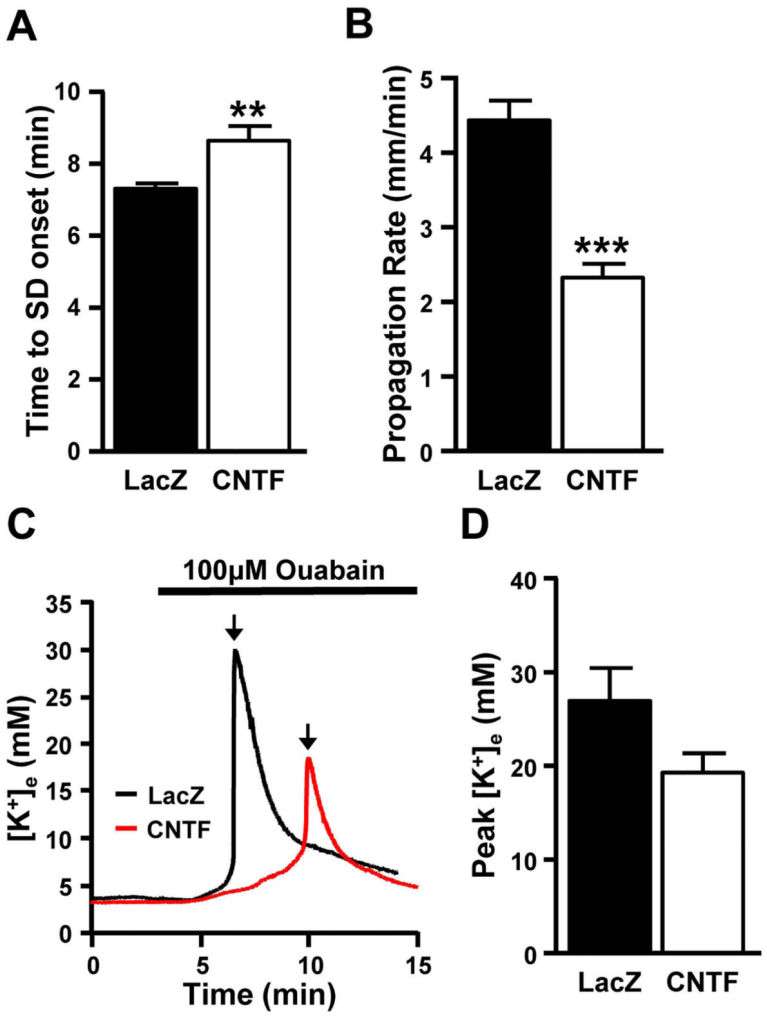

Figure 5. Contribution of Na^+/K^+-ATPase pump in the reduced susceptibility to SD of CNTF tissues

During 100 μM ouabain exposures, both electrical recordings and intrinsic optical signals were used to measure SD in the *sr* of the CA1. **A.** Although SD could be induced in all CNTF preparations (n=12), the latency to SD was significantly longer when compared to LacZ controls (n=12) (t(22)=3.12, **p=.005, independent t-test). **B.** The rate of propagation was also significantly slower in CNTF preparations when compared to LacZ slices (n=12, t(22)=6.53, ***p<.0001, independent t-test). **C.** Examples of K^+ responses (in mM) from a LacZ preparation (black) and a CNTF preparation (red) during SD induced by 100 μM ouabain. Black arrows indicate SD onset. **D.** Extracellular changes in K^+ were measured during ouabain-induced SD. While not significant, there was a trend towards a decrease in the peak concentration of extracellular K^+ in CNTF preparations compared with LacZ controls (n=12, (t(22)=1.887, p=.0724, independent t-test)).

Table 1

Primer sequences for qPCR analysis

GENE	DIRECTION	SEQUENCE
mouse *ATP1alpha2*	Forward	AGTGAGGAAGATGAGGGACAGG
	Reverse	GTTCCCCAAGTCCTCCCAGC
mouse *Cyclophilin A*	Forward	ATGGCAAATGCTGGACCAAA
	Reverse	GCCTTCTTTCACCTTCCCAAA
mouse *GFAP*	Forward	ACGACTATCGCCGCCAACT
	Reverse	GCCGCTCTAGGGACTCGTTC
mouse *KIR4.1*	Forward	AGAGGGCCGAGACGAT
	Reverse	TTGACCTGGTTGAGCCGAATA
mouse *NKCC1*	Forward	TTGGCTGGATCAAGGGTGTAT
	Reverse	CTCTGCGAATCCGACAACA